S100A8/A9 Promotes Dendritic Cell–Mediated Th17 Cell Response in Sjögren's Dry Eye Disease by Regulating the Acod1/STAT3 Pathway

Yankai Wei, Mei Sun, Xinyu Zhang, Chengyuan Zhang, Chao Yang, Hong Nian, Bei Du, and Ruihua Wei

Tianjin Key Laboratory of Retinal Functions and Diseases, Tianjin Branch of National Clinical Research Center for Ocular Disease, Eye Institute and School of Optometry, Tianjin Medical University Eye Hospital, Tianjin, China

Correspondence: Ruihua Wei, Tianjin Key Laboratory of Retinal Functions and Diseases, Tianjin Branch of National Clinical Research Center for Ocular Disease, Eye Institute and School of Optometry, Tianjin Medical University Eye Hospital, 251 Fukang Rd., Nankai District, Tianjin 300384, China; rwei@tmu.edu.cn.

YW and MS equally contributed to the work.

Received: September 27, 2024
Accepted: December 19, 2024
Published: January 14, 2025

Citation: Wei Y, Sun M, Zhang X, et al. S100A8/A9 promotes dendritic cell–mediated Th17 cell response in Sjögren's dry eye disease by regulating the Acod1/STAT3 pathway. *Invest Ophthalmol Vis Sci.* 2025;66(1):35. https://doi.org/10.1167/iovs.66.1.35

Purpose. To investigate the role of S100A8/A9 in the pathogenesis of Sjögren's dry eye disease (SjDED) and explore its potential mechanism of action.

Methods. S100A8/A9 expression was determined by western blot and quantitative real-time polymerase chain reaction (qRT-PCR). Tear secretion, corneal fluorescein staining, and hematoxylin and eosin staining were used to evaluate the effect of paquinimod, a S100A8/A9 inhibitor, on dry eye disease in nonobese diabetic (NOD) mice. Immune cell infiltration and percentage were assessed by immunofluorescence and flow cytometry. Proinflammatory cytokine levels were examined by qRT-PCR or ELISA. The mechanism of action was analyzed using western blot, immunofluorescence, and chromatin immunoprecipitation.

Results. S100A8/A9 was upregulated in peripheral blood mononuclear cells of patients with SjDED and lacrimal glands (LGs) of SjDED mice. The upregulation of S100A8/A9 was correlated with the dry eye severity and inflammatory infiltration levels in LGs. Administration of paquinimod ameliorated clinical and histopathological phenotypes of SjDED mice and reduced the proportion of Th17 cells in LGs, lymph nodes, and spleens. Further experiments revealed that S100A8/A9 did not directly affect Th17 generation and function but upregulated the expression of major histocompatibility complex II (MHC II) and Th17-polarizing cytokines in dendritic cells (DCs) to augment Th17 cell response. Mechanistically, S100A8/A9 induced the expression of Acod1 and thereby promoted the activation and nuclear translocation of signal transducer and activator of transcription 3 (STAT3), resulting in increased *Il23a* transcription. STAT3 activator reversed the therapeutic effect of paquinimod on SjDED mice.

Conclusions. S100A8/A9 activated the Acod1/STAT3 pathway to promote DC-driven Th17 cell responses in SjDED. The S100A8/A9/Acod1/STAT3 pathway may represent a promising therapeutic target for SjDED.

Keywords: Sjögren's dry eye disease, Th17 cell, S100A8/A9, dendritic cell

Sjögren's dry eye disease (SjDED) is a chronic autoimmune eye disorder characterized by the infiltration of lymphocytes and myeloid cells into the lacrimal glands (LGs) and ocular surface, which can cause gland dysfunction, ocular discomfort and even vision loss.[1] The conventional steroids can reduce ocular surface inflammation, but long-term use is often linked to some undesirable side effects, including increased intraocular pressure and development of cataract.[2] Recently, the use of immunosuppressive agents and biologics has helped to reduce the use of corticosteroids.[1,3] Nonetheless, the limited effectiveness of immunosuppressive and biological reagents highlights the need for better understanding of the pathogenesis of SjDED. Currently, increasing evidence indicates that Th17 cells are a significant contributor to the onset and progression of SjDED.[4,5] Inhibition of the Th17 cell response has been demonstrated to be an effective tactic for mitigating SjDED.[6] Therefore, studies to clarify the mechanisms involved in the Th17 cell program are imperative to develop additional and more effective therapeutic agents for the treatment of SjDED.

The differentiation and function of Th17 cells are regulated by multiple extracellular and intracellular signals.[7] Among them, dendritic cell (DC)-derived immune signals, especially the polarizing cytokines IL-6, IL-23, and IL-1β, can instruct naïve T cells to develop into Th17 cells.[7] Furthermore, DCs are capable of upregulating major histocompatibility complex II (MHC II) and costimulatory molecules, such as CD80 and CD40, to promote the activation and proliferation of Th17 cells.[8] It has been shown that multiple factors, including danger-associated molecular patterns, cytokines, and transcription factors, contribute to determining the expression of Th17-polarizing molecules in DCs.[9,10] Among them, the transcription factor signal trans-

ducer and activator of transcription 3 (STAT3) is implicated as a key player in the maturation and function of DCs,[11] but the roles of STAT3 in DC-mediated Th17 cell response and the upstream molecules that regulate STAT3 are still not clear.

The calcium-binding proteins S100A8 and S100A9 belong to the S100 family and often form heterodimers (S100A8/A9) that are mainly expressed on myeloid cells, including neutrophils, monocytes, and DCs.[12] In recent years, S100A8/A9 has gained increasing interest as a critical damage-associated molecular pattern molecule or alarmin.[13] After its release, S100A8/A9 binds to its receptor and induces the production of myriad cytokines, chemokines, and adhesion factors, thereby initiating and amplifying immune responses.[14] It has been demonstrated that S100A8/A9 was significantly upregulated in the tears of patients with dry eye disease (DED) and LGs of dry environment–induced DED rat models.[15–17] Most recently, Liang et al.[18] reported that S100A9 was upregulated in the corneal epithelia of the LG excision model and suppressed autophagy through activation of Toll-like receptor 4 (TLR4) in DED. Furthermore, an increase in S100A8/A9 level was observed in the conjunctiva of SjDED patients and tears of the SjDED rabbit model,[19,20] indicating a potential association between S100A8/A9 and SjDED. Nevertheless, the precise role of S100A8/A9 in the pathogenesis of SjDED remains unclear.

In 2010, it was reported that S100A8/A9 was required for the development of autoreactive $CD8^+$T cells and could induce IL-17 production by $CD8^+$T cells from patients with systemic lupus erythematosus and mouse models.[21] Recently, Yun and colleagues[22] observed that the $CD4^+$ $IL\text{-}17^+$ cell percentage and IL-17 production were significantly reduced in T cells from experimental autoimmune uveitis rats treated with S100A8/A9 inhibitor. In addition, Defrêne et al.[23] demonstrated that $S100A8^{-/-}$ and $S100A9^{-/-}$ mice exhibited more severe psoriasis symptoms than wild-type (WT) mice, accompanied by elevated IL-17A and IL-17F production by $CD4^+$T cells. These findings indicate that S100A8/A9 may have an impact on the differentiation and function of Th17 cells. Nevertheless, whether S100A8/A9 regulates Th17 cell response in the context of SjDED and the downstream mechanisms is yet to be determined.

In this study, we investigated the role of S100A8/A9 in the pathogenesis of SjDED, especially its regulation of Th17 cell responses. We demonstrated that the expression of S100A8/A9 was elevated in peripheral blood mononuclear cells (PBMCs) of patients with SjDED and LGs of the SjDED mouse model. Inhibiting S100A8/A9 could effectively ameliorate the development of SjDED by suppressing Th17 cell responses. Mechanistically, S100A8/A9 induced the expression of *Il23a* and MHC II in DCs by activating Acod1/STAT3 signaling, which promoted Th17 cell response and finally led to the progression of SjDED. Thus, our research unveiled a previously unidentified role for S100A8/A9 in DC-mediated Th17 cell responses during SjDED and indicate that S100A8/A9 might represent a potential therapeutic target for the management of SjDED.

Methods

Patients

This study was conducted at Tianjin Medical University Eye Hospital (Tianjin, China). Seven patients diagnosed with non-SjDED (female; mean age, 59.5 ± 8.54 years) and eight patients diagnosed with SjDED (female; mean age, 62.13 ± 9.25 years) were involved. All patients were required to meet the diagnostic criteria for DED as outlined in the TFOS DEWS II report.[24] Furthermore, the patients diagnosed with SjDED were required to meet the 2016 revised Sjögren's disease (SjD) criteria proposed by the American-European Consensus Group,[25] including exhibiting anti-Ro/SSA antibody positivity, an ocular staining score of at least 5 points, and a Schirmer's test result of ≤5 mm per 5 minutes. Peripheral blood was collected from the enrolled patients and processed with Ficoll gradient centrifugation to isolate PBMCs. All human participants were enrolled using protocols approved by the Ethics Committee Review Board of Tianjin Medical University Eye Hospital (2021KY-17), and written informed consent was obtained from participants. This study adhered to the tenets of the Declaration of Helsinki.

Mice

Nonobese diabetic (NOD)/ShiLtJ mice and BALB/c mice were purchased from GemPharmatech Co., Ltd. (Nanjing, China) and raised under pathogen-free conditions in the animal facilities of Tianjin Medical University Eye Hospital. Sex- and age-matched (4–24 weeks of age) mice were used for the experiments. All animal experiments were performed in accordance with the standards of the ARVO Statement on the Use of Animals in Ophthalmic and Vision Research and approved by the Institutional Animal Care and Use Committee of Tianjin Medical University Eye Hospital.

Reagents, Cytokines, and Antibodies

Paquinimod (S100A8/A9 inhibitor, T7310; TargetMol Chemicals, Boston, MA, USA) was dissolved in dimethyl sulfoxide (DMSO; Solarbio, Beijing, China) for storage and use. Recombinant mouse S100A8/A9 (8916-S8), TGF-β (7666-MB), IL-6 (406-ML), IL-23 (1887-ML), IL-4 (404-ML), and granulocyte–macrophage colony-stimulating factor (GM-CSF; 415-ML) were purchased from R&D Systems (Minneapolis, MN, USA). Antibodies to CD3 (16-0031-86), CD28 (16-0281-86), and neutralizing antibodies to IL-4 (16-7041-85), IFN-γ (16-7312-85), and IL-23 p19 (14-7232-85) were purchased from eBioscience (San Diego, CA, USA). The antibodies used in the flow cytometry and western blot analysis, as well as their dilution ratio, can be found in Supplementary Table S1.

Administration of S100A8/A9 Inhibitor

We first measured the body weight of NOD mice and assessed the extent of DED using tear secretion levels and corneal fluorescein staining scores. NOD mice with similar body weight and DED severity were paired, randomly grouped by assigning a random number to each mouse according to a random number table, and intraperitoneally (IP) injected with S100A8/A9 inhibitor paquinimod (25 mg/kg) or equal volume of solvent every other day for 4 weeks starting at 16 weeks of age when SjD-like autoimmune dacryoadenitis was fully established. BALB/c WT mice were used as healthy controls in this study. NOD and BALB/c mice were euthanized at 28 days after treatment to collect different tissues (such as LGs, spleens, and lymph nodes) and examine histopathological changes.

Investigative Ophthalmology & Visual Science

Drug Rescue Assay

The NOD mice were randomly divided into three groups for the STAT3 agonist colivelin rescue assay. One group was IP administered 25 mg/kg of paquinimod every other day, and, on days 14 and 21 after paquinimod administration, the same mice were given 2 mg/kg of colivelin (sc-361153; Santa Cruz Biotechnology, Dallas, TX, USA). The second group was administered 25 mg/kg of paquinimod every other day, without the additional injection of colivelin. The control group was treated with an equal volume of solvent.

Phenol Red Thread Test

To quantify the tear secretion, phenol red cotton threads (Jingming Co., Ltd., Tianjin, China) were gently held in the lower conjunctival fornix at one-third of the lower eyelid distance from the lateral canthus for 30 seconds in each eye. The length of thread wetting was measured and expressed in millimeters. Each eye was examined and recorded three times, and the average wetting length was determined as the final length.

Fluorescein Ocular Surface Staining

To assess the corneal epithelial defects, each eye of the mice was instilled with 1 µL of 2% sodium fluorescein in the lateral conjunctival sac before three artificial blinks. After 90 seconds, corneas were examined and photographed using a MICRON IV biomicroscope (Phoenix Research Labs, Pleasanton, CA, USA) under a cobalt blue light. The scoring of cornea epithelial staining was performed in a masked manner using the criteria described by Xiao et al.[26]

Histologic Analysis of Lacrimal Glands

The NOD mice were sacrificed at the end of the experiment, and LGs were harvested carefully from these mice, fixed in 10% formalin, and embedded in paraffin. Then, 5-µm-thick LG sections were cut and stained with hematoxylin and eosin (H&E). Conventional light microscopy (BX51 fluorescence microscope; Olympus Corporation, Tokyo, Japan) was applied to capture images of the LG tissues stained with H&E. Inflammation of the LGs was evaluated blindly by examining three nonconsecutive whole-gland cross-sections and were quantified by standard focus scoring. A focus was defined as an aggregate of at least 50 lymphocytes, and the focus score was defined as the number of foci per 4 mm^2 of LGs from each group. The LG tissue area was quantified using ImageJ software (National Institutes of Health, Bethesda, MD, USA).[27,28]

$CD4^+$T Cell Isolation and Polarization

$CD4^+$T cells were isolated from spleens and lymph nodes of NOD mice and enriched by positive selection using PE anti-mouse CD4 antibody, Anti-PE MicroBeads (130-048-801; Miltenyi Biotec, Bergisch Gladbach, Germany), and a MACS Separator (Miltenyi Biotec). To determine the direct effect of S100A8/A9 on Th17 cells (Tregs), purified T cells were seeded in 24-well plates (8×10^5 cells per well) and incubated with recombinant S100A8/A9 protein (R&D Systems) or vehicle in the presence of anti-CD3 (5 µg/mL) and anti-CD28 (5 µg/mL). For Th17 polarization, 10 µg/mL anti–IL-4, 10 µg/mL anti–IFN-γ, 5 ng/mL TGF-β, 40 ng/mL IL-6, and 20 ng/mL IL-23 were added into the culture medium. The polarized cells were supplemented with fresh medium containing cytokines as needed. After 3 or 4 days, cells were collected for flow cytometry analysis, and the culture supernatants were subjected to ELISA analysis.

Generation and Transfection of Bone Marrow–Derived DCs

Mouse bone marrow–derived dendritic cells (BMDCs) were induced as described by Inaba et al.[29] Briefly, bone marrow cells were isolated from femurs and tibiae of NOD mice and cultured in complete RPMI 1640 medium supplemented with GM-CSF (10 ng/mL) and IL-4 (10 ng/mL). On day 3, the medium was changed to fresh medium containing GM-CSF and IL-4. On day 6, BMDCs were collected for subsequent experiments. Transfection of BMDCs with small interfering RNA (siRNA) targeting Acod1 (GenePharma, Suzhou, China) was performed according to the methods described by us previously.[30] The siRNA sequence targeting Acod1 is 5′-AUCAUUCGGAGGAGCAAGATT-3′ (sense) and 5′-UCUUGCUCCUCCGAAUGAUACTT-3′ (antisense). The sequence of negative control was 5′-UUCUCCGAACGUGUCACGUTT-3′ (sense) and 5′-ACGUGACACGUUCGGAGAATT-3′ (antisense).

Co-Culture of $CD4^+$T Cells and DCs

DCs treated with S100A8/A9 or vehicle were washed and co-cultured with $CD4^+$T cells prepared from NOD mice at the ratio of 1:20 under Th17-polarizing condition. Then, 48 or 72 hours later, cells were harvested and subjected to quantitative real-time polymerase chain reaction (qRT-PCR) and flow cytometry analysis.

Carboxyfluorescein Succinimidyl Ester Staining Assay

The carboxyfluorescein succinimidyl ester (CFSE) staining assay was used to measure T-cell proliferation. Briefly, cells sorted from the spleen and lymph nodes of NOD mice were washed and resuspended at 1×10^7/mL in PBS containing 1-µM CFSE (Thermo Fisher Scientific, Waltham, MA, USA). After incubation in CFSE at 37°C for 10 minutes, T cells were washed, suspended with RPMI 1640 medium containing 10% fetal bovine serum (FBS), and then co-cultured with S100A8/A9- or vehicle-treated DCs at a ratio of 1:20 under Th17-polarizing condition. After 72 hours, flow cytometry was used to analyze T-cell proliferation.

RNA Sequencing and Data Analysis

The RNA sequencing (RNA-seq) libraries were constructed by E-GENE Co., Ltd. (Shenzhen, China) as follows. Briefly, total RNAs of vehicle- or S100A8/A9-treated BMDCs were extracted using Invitrogen TRIzol Reagent (Thermo Fisher Scientific) and then treated with RNase-free DNase I for 30 minutes according to the manufacturer's protocols. The poly(A)-containing mRNA was purified using oligo(dT) beads from the total RNA and then fragmented into 100 to 200 nucleotides using divalent cations at an elevated temperature. The fragmented mRNA was reverse transcribed with SuperScript II Reverse Transcriptase (Thermo Fisher Scien-

Investigative Ophthalmology & Visual Science

tific) and further extended into double-stranded cDNA using ribonuclease H (RNaseH) and DNA polymerase I (Pol I) by random priming. The cDNA was subsequently adapter ligated with unique indices and amplified following PCR. The libraries were analyzed by an Agilent 4200 TapeStation system (Agilent Technologies, Santa Clara, CA, USA) and quantified by qPCR before being sequenced on the Illumina sequencing platform.

For RNA–seq analysis, FastQC 0.11.5 software was used to perform quality control of raw reads. The clean reads were obtained following the removal of low-quality reads with Trimmomatic 0.38 software and then aligned to the *Mus musculus* genome reference (UCSC mm10) using Hisat2 2.2.1 software. TPM (transcripts per kilobase of exon model per million mapped reads) values were calculated by StringTie 2.1.7 based on the number of reads and were used to estimate the expressed values. DEseq2 1.34.0 was applied to calculate the differential expression of TPM values. Kyoto Encyclopedia of Genes and Genomes (KEGG) enrichment analysis was performed using DAVID (https://david.ncifcrf.gov/).

ELISA

Supernatant IL-17 levels were measured using a Mouse IL-17 DuoSet ELISA Kit (DY421; R&D Systems) according to the manufacturer's protocol. The chromogenic signal was developed using a Substrate Reagent Pack (DY999; R&D Systems), and the absorbance was measured at 450 nm with a reference wavelength of 540 nm using a Spark 10 M luminometer (Tecan, Männedorf, Switzerland).

Flow Cytometry

For surface marker staining, single-cell suspensions were pretreated with Fc block antibody (156604; BioLegend, San Diego, CA, USA) for 15 minutes and stained with FITC- or PE-conjugated antibodies, including anti-mouse CD4, CD11c, CD40, CD80, and MHC II antibodies, for 20 minutes at 4°C. For intracellular staining, cells were resuspended in complete RPMI 1640 medium containing phorbol myristic acetate (50 ng/mL), ionomycin (1 µg/mL), and brefeldin A (1 µg/mL), all obtained from Sigma-Aldrich (St. Louis, MO, USA). They were then incubated at 37°C for 4 hours. The cells were washed, fixed, and permeabilized overnight with an eBioscience Intracellular Fixation & Permeabilization Buffer Set, followed by intracellular staining with allophycocyanin-, FITC-, or PE-conjugated antibodies against IFN-γ, IL-17, or Foxp3 for 2 hours. Data from stained cells were acquired using a flow cytometer (FACS Calibur; BD Biosciences, San Jose, CA, USA) and analyzed with FlowJo software.

Quantitative Real-Time PCR

Total RNA was extracted from the cells and LGs with the EZ-press RNA Purification Kit (EZBioscience, Roseville, MN, USA), followed by reverse transcription using the RevertAid First Strand cDNA Synthesis Kit (Thermo Fisher Scientific) according to the manufacturer's instructions. qRT-PCR was conducted using FastStart Universal SYBR Green Master (04913914001; Roche, Basel, Switzerland) on a Roche LightCycler 480 Real-Time PCR system. Relative expression differences between experimental samples and controls were calculated based on the $2^{-\Delta\Delta Ct}$ method with reference to glyceraldehyde-3-phosphate dehydrogenase (GAPDH). For a detailed list of primer sequences used for qRT-PCR, please see Supplementary Table S2.

Western Blotting Analysis

Samples were lysed with RIPA Lysis Buffer (Beyotime, Shanghai, China) containing phenylmethylsulfonyl fluoride (PMSF; Solarbio) and phosphatase inhibitor cocktail (Cell Signaling Technology, Danvers, MA, USA). The protein concentration was measured using a Solarbio BCA Protein Assay Kit. The whole lysates were boiled in loading buffer at 100°C for 10 minutes, and equal amounts of protein were applied to electrophoresis on 8% or 12% sodium dodecyl sulfate–polyacrylamide gel electrophoresis (SDS-PAGE) gel and transferred onto a polyvinylidene difluoride (PVDF) membrane. After blocking with 5% nonfat milk for 2 hours to minimize non-specific binding, the membranes were incubated overnight at 4°C with primary antibodies to phospho-JAK2 (p-JAK2, 1:1000), JAK2 (1:1000), phospho-STAT3 (p-STAT3, 1:2000), STAT3 (1:1000), phospho-Akt (p-Akt, 1:1000), S100A8 (1:500), S100A9 (1:500), and β-actin (1:2000). The following day, the membranes were incubated with horseradish peroxidase (HRP)-conjugated secondary antibody (1:1000) for 2 hours at room temperature. The protein bands were visualized by using ECL reagent (Cytiva, Marlborough, MA, USA) and scanned with a 4800 Chemiluminescent Imaging System (Tanon Co., Ltd., Shanghai, China). Western blot quantification was performed by ImageJ software.

Immunofluorescence

LG tissue immunofluorescence was carried out as we previously described.[31] For cell immunofluorescence, BMDCs treated with or without recombinant S100A8/A9 protein were collected and fixed with 4% paraformaldehyde for 15 minutes at room temperature on a microscope slide and washed by phosphate-buffered saline with Triton (PBST, P1031; Solarbio). After blocking in 5% goat serum (SL038; Solarbio) in PBST for 1 hour, samples were incubated with anti–p-STAT3 antibody (9145, 1:100; Cell Signaling Technology) overnight at 4°C and then stained with Goat Anti-Rabbit IgG H&L (Alexa Fluor 647) (ab150079, 1:500; Abcam, Cambridge, UK) for 2 hours at room temperature. Subsequently, the nuclei were stained with 4′,6-diamidino-2-phenylindole (DAPI; Sigma-Aldrich for 15 minutes, and images were captured using a LSM 800 confocal microscope (ZEISS, Oberkochen, Germany) with a 63× oil immersion objective.

Chromatin Immunoprecipitation Assay

The chromatin immunoprecipitation (ChIP) assay was conducted with a ChIP Kit (ab500; Abcam). Briefly, DC2.4 cells treated with or without recombinant S100A8/A9 protein were collected and cross-linked with 1% formaldehyde for 10 minutes at room temperature before termination with 125-mM glycine. Subsequently, samples were suspended in lysis buffer and sonicated to obtain 200- to 1000-bp DNA fragments. The antibody against p-STAT3 (9145, 5 µg; Cell Signaling Technology) was used to immunoprecipitate the protein–DNA complexes. The next day, the immunoprecipitated DNA was pulled using Protein A Agarose beads through incubation with rotation for 1 hour at 4°C and

Investigative Ophthalmology & Visual Science

then was purified using DNA purifying slurry. qRT-PCR was performed to measure the enrichment of STAT3 on the *Il23a* promotor region using the primer sequences listed in Supplementary Table S3.

Data Availability

RNA-seq data generated in this study are deposited in the NCBI Gene Expression Omnibus (GEO) database (accession no. GSE276800). ChIP-seq data are available in the GEO database under accession no. GSE36099 and GSE27161. The microarray profiles were downloaded from the GEO database (accession no. GSE176510).

Statistics

Graphs were generated and statistically analyzed with Prism 8 (GraphPad Software, Boston, MA, USA). The normal distribution of the data was tested by the Shapiro–Wilk test. Comparisons between two groups were analyzed using two-tailed Student's *t*-test and Mann–Whitney test depending on the normality of the data. For more than two groups, one-way ANOVA, two-way ANOVA, and Kruskal–Wallis test were used to analyze the variance according to the data normality. The Spearman correlation test was used to assess the correlation between two variables. All data are shown as mean ± SD. Data shown are representative of experiments that were repeated three or more times, including cell experiments, animal studies, and blots. Significance is indicated as $^{*}P < 0.05$ or $^{**}P < 0.01$ (ns, no significance).

Results

Expression Levels of S100A8 and S100A9 Are Elevated in LGs of SjDED Mice and PBMCs of SjDED Patients

NOD/LtJ mice are one of the most common animals used in primary SjD models due to their SjD-like manifestations, such as autoimmune dacryoadenitis and sialadenitis. Our results of corneal fluorescein staining, tear secretion, and LGs histology indicate that the severity of DED increased with age in mice between the ages of 4 and 16 weeks but was relatively stable in mice between the ages of 16 and 24 weeks (Supplementary Figs. S1A–S1E). To determine the changes in S100A8 and S100A9 expression during the development of SjDED, LGs were isolated from 4-, 8-, 12-, and 16-week-old NOD mice, and S100A8 and S100A9 expression was detected. The results showed that the expression of S100A8 and S100A9 was significantly elevated in LGs of NOD mice with increasing age at the mRNA and protein levels (Figs. 1A, 1B). By employing Spearman correlation analysis, we further found that the expression levels of S100A8 and S100A9 were positively correlated with the extent of inflammatory cell infiltration in LGs (Fig. 1C).

We next sought to identify the expression of S100A8 and S100A9 in patients with SjDED by isolating PBMCs. As seen in Figure 1D, the expression of S100A8 and S100A9 was significantly higher in PBMCs of patients with SjDED than in non-SjDED patients. The increased levels of S100A8 and S100A9 were positively correlated with the Ocular Surface Disease Index (OSDI) scores and negatively correlated with tear secretion (Figs. 1E–1H). Furthermore, we observed that the mRNA levels of S100A8 and S100A9 were also upregulated in the conjunctiva of patients with SjD keratoconjunctivitis sicca compared with healthy individuals by analyzing a published microarray dataset (GSE176510) (Fig. 1I). Taken together, these results suggest that S100A8 and S100A9 are upregulated in PBMCs of SjDED patients and LGs of SjDED mice, which is closely associated with the severity of SjDED.

Inhibiting S100A8/A9 Efficiently Alleviates SjDED in NOD Mice by Suppressing Th17 Cell Responses

To investigate whether inhibiting S100A8/A9 has a therapeutic effect on SjDED, we IP injected S100A8/A9 inhibitor paquinimod or an equal volume of vehicle into 16-week-old NOD mice every other day for 28 days (Fig. 2A). As seen in Figures 2B and 2C, the vehicle-treated SjDED mice displayed aggravated corneal fluorescein staining compared to the WT mice, whereas the application of paquinimod led to a significant decrease in corneal epithelial staining as early as 14 days after treatment, and this effect was maintained until 28 days after paquinimod administration. Furthermore, tear production was significantly increased in the paquinimod-treated group compared to the vehicle-treated group (Fig. 2D). The attenuated effect was also observed in histological images, which displayed less infiltration of inflammatory cells in LGs of paquinimod-treated mice than in vehicle-treated mice (Fig. 2E). Therefore, these data suggest that paquinimod reduces the clinical severity of DED and LG inflammation in NOD mice.

Given that Th17 cells are central to the pathogenesis of SjDED, we next sought to determine if the therapeutic effects of paquinimod on SjDED were because of altered Th17 cell responses. For this, the LGs of paquinimod- or vehicle-treated mice were collected at day 28 posttreatment and subjected to immunofluorescence analysis. The results showed that, after treatment with paquinimod, $CD4^{+}IL\text{-}17^{+}$ cell infiltration was significantly decreased in LGs of SjDED mice (Fig. 2F). Consistent with this, flow cytometry analysis revealed a reduced frequency of Th17 cells in spleens and lymph nodes from paquinimod-treated mice compared to those in vehicle-treated mice (Figs. 2G, 2H), but the frequency of Tregs was elevated in spleens of paquinimod-treated mice (Supplementary Fig. S2A). In addition, the percentages of Tregs in lymph nodes and the percentages of Th1 cells in lymph nodes and spleens from paquinimod-treated mice were comparable to those in vehicle-treated mice (Supplementary Figs. S2B–S2D). Collectively, these results indicate that paquinimod can efficiently inhibit Th17 cell responses to mitigate SjDED.

S100A8/A9 Promotes Th17 Cell Responses Through Its Action on DCs

Having observed the effect of S100A8/A9 inhibitor on Th17 cells in vivo, we next determined the regulation of S100A8/A9 on the differentiation and function of Th17 cells in vitro. To this end, $CD4^{+}$T cells purified from the spleen and lymph nodes of NOD mice were cultured in the presence or absence of recombinant S100A8/A9 protein under Th17-polarizing conditions. Then, 72 hours later, intracellular expression of IL-17 in T cells was analyzed by flow cytometry, and IL-17 secretion in the supernatant was detected by ELISA. The results showed that the percentages of $CD4^{+}IL\text{-}17^{+}$ T cells and IL-17 production were not significantly different between the S100A8/A9- and vehicle-treated groups

Investigative Ophthalmology & Visual Science

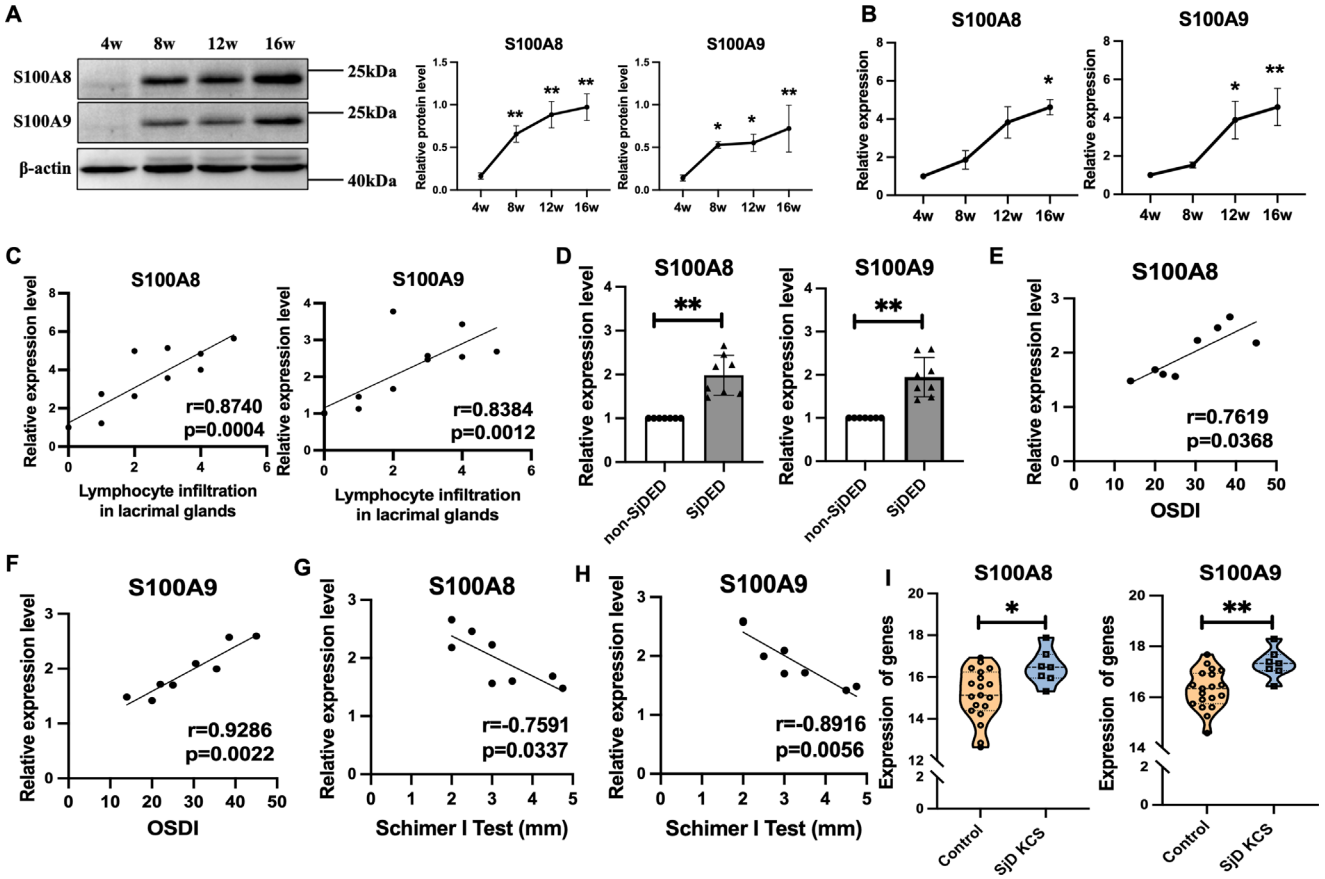

Figure 1. The expression levels of S100A8 and S100A9 are elevated in LGs of SjDED mice and PBMCs of SjDED patients. (**A**) Immunoblot analysis of S100A8 and S100A9 in LGs from 4-, 8-, 12-, and 16-week-old NOD mice ($n = 3$ per group). (**B**) qRT-PCR analysis of S100A8 and S100A9 expression at the mRNA level in LGs of 4-, 8-, 12-, and 16-week-old NOD mice ($n = 4$ per group). (**C**) Correlation between the expression of S100A8/A9 and the extent of inflammatory cell infiltration in LGs of 4-, 8-, 12-, and 16-week-old NOD mice ($n = 12$). (**D**) qRT-PCR analysis of S100A8 and S100A9 mRNA expression in PBMCs from patients with non-SjDED ($n = 7$) and those with SjDED ($n = 8$). (**E**, **F**) Correlation between the expression of S100A8/A9 and OSDI scores in SjDED patients ($n = 8$). (**G**, **H**) Correlation between the expression of S100A8/A9 and the tear secretion levels in SjDED patients ($n = 8$). (**I**) Analysis of S100A8 and S100A9 expression in the conjunctiva of patients with Sjögren's disease keratoconjunctivitis sicca (SjD KCS; $n = 7$) compared with healthy individuals (control, $n = 19$) using GEO dataset GSE176510. One-way ANOVA test (**A**), Kruskal–Wallis test (**B**), Mann–Whitney test (**D**), and two-tailed Student's *t*-test (**I**) were used to assess statistical significance. The correlation analysis used in (**C**) and (**E**–**H**) was Spearman's correlation. Data are reported as mean ± SD. $^{*}P < 0.05$, $^{**}P < 0.01$.

(Figs. 3A, 3B), suggesting that the inhibitory effect of paquinimod on Th17 cells observed in vivo was not due to a direct effect on T cells. DCs are professional antigen-presenting cells (APCs) that can direct the differentiation of naïve $CD4^+$T cells into Th17 cells, so we next investigated whether S100A8/A9 acted on DCs to regulate Th17 cell responses. To confirm this, BMDCs were preincubated with recombinant S100A8/A9 protein for 24 hours, washed, and then co-cultured with $CD4^+$T cells under Th17-polarizing conditions. As shown in Figure 3C, pretreatment of DCs with S100A8/A9 resulted in a higher proportion of Th17 cells. In agreement with the flow cytometry findings, T cells co-cultured with S100A8/A9-treated DCs exhibited increased IL-17 secretion and expression of Th17-related genes, including *Il17a*, *Il17f*, and *RORγt* (Figs. 3D–3G). Moreover, T-cell proliferation was evaluated using CFSE staining. The results showed that Th17 cells co-cultured with S100A8/A9-treated DCs proliferated faster than those in the control group (Fig. 3H). Thus, these data strongly suggest that S100A8/A9 acts on DCs but not directly on $CD4^+$T cells to regulate Th17 cell generation and function.

S100A8/A9 Promotes the Maturation and Function of DCs

DC-derived costimulatory molecules and cytokines are crucial for the activation and differentiation of Th17 cells.[7,8] Because our previous results showed that S100A8/A9 promoted DC-driven Th17 responses, we investigated whether it affected DC maturation and function. Flow cytometry results showed that S100A8/A9 significantly increased MHC II expression in DCs, but no significant differences in CD40 and CD80 expression were observed between S100A8/A9- and vehicle-treated DCs (Fig. 4A). We also investigated the profiles of inflammatory genes in S100A8/A9-stimulated DCs. The mRNA expression of Th17-polarizing cytokines (including *Il6*, *Il23a* and *Il1b*) and pro-inflammatory chemokines (including *Cxcl1*, *Cxcl2* and *Cxcl3*) was significantly increased in S100A8/A9-stimulated DCs compared to the control group (Figs. 4B, 4C), whereas the expression level of *Il12a* was not significantly different (Fig. 4D). Furthermore, we used anti–IL-23p19 antibodies to explore whether blocking IL-23 could

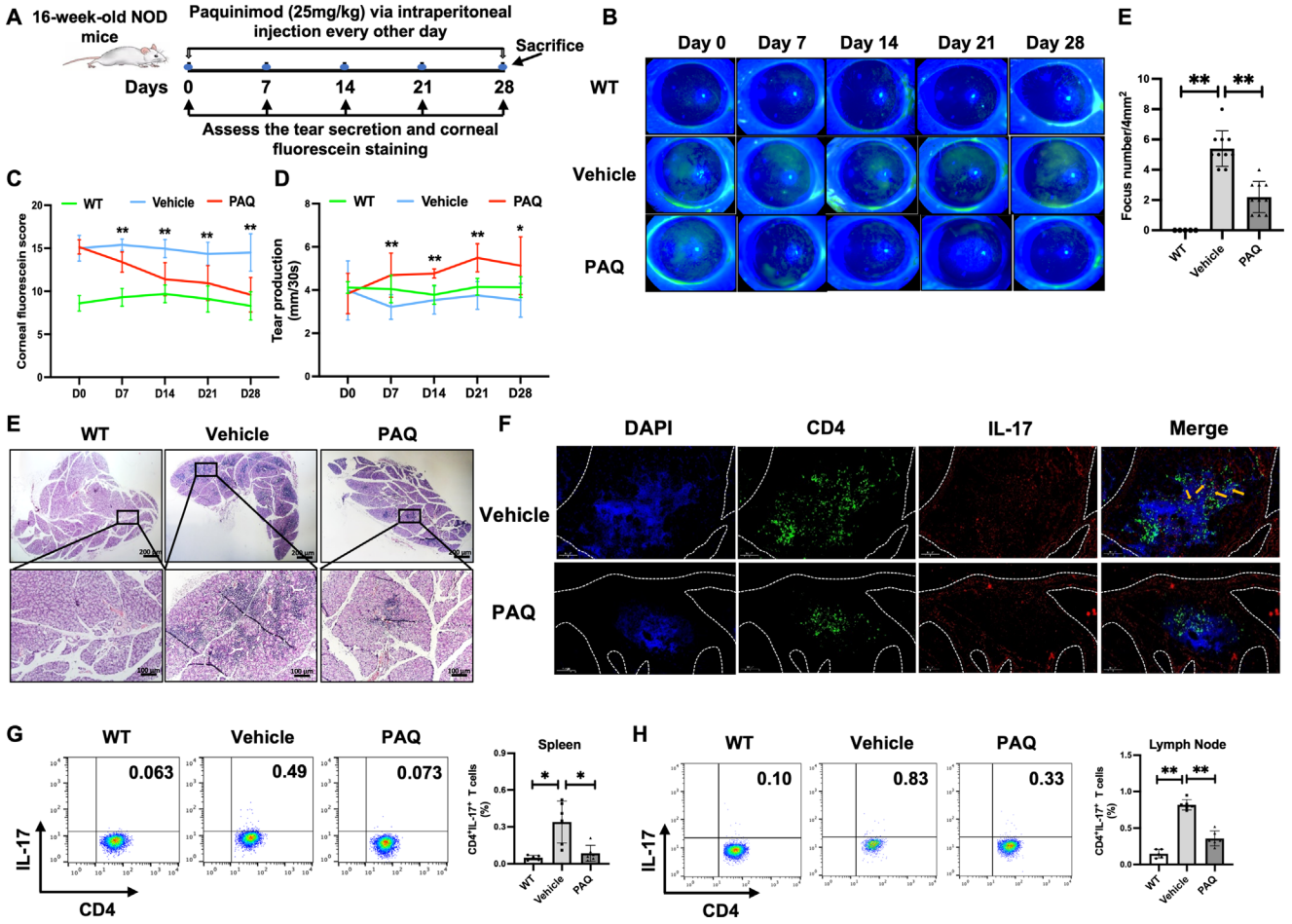

Figure 2. Paquinimod ameliorates SjDED in NOD mice by inhibiting Th17 cell responses. (**A**) The schematic for the treatment of NOD mice by intraperitoneal injection of paquinimod (PAQ) or vehicle. (**B–D**) The representative images (**B**), grading scores of corneal fluorescein staining (**C**), and tear secretion levels measured by phenol red cotton threads (**D**) in WT BALB/c mice ($n = 5$), vehicle-treated and PAQ-treated NOD mice with SjDED ($n = 10$). (**E**) Representative images and histological scoring of H&E-stained sections showing the extent of lymphocytic infiltration in LGs of WT mice ($n = 5$) and vehicle- and PAQ-treated mice ($n = 10$) at the end of the experiment. *Scale bar*: 200 µm (upper panels); 100 µm (lower panels). (**F**) Immunofluorescence analysis for $CD4^+IL\text{-}17^+$ cells in lacrimal gland sections of vehicle-treated and PAQ-treated NOD mice ($n = 3$). *Yellow arrows* represent $CD4^+IL\text{-}17^+$ cells. *Scale bar*: 100 µm. (**G**, **H**) Flow cytometric analysis of the percentages of $CD4^+IL\text{-}17^+$ cells in spleens (**G**) and lymph nodes (**H**) of WT, vehicle-treated, and PAQ-treated mice ($n = 5$ or 6). Two-way ANOVA test (**C**, **D**), Kruskal–Wallis test (**E**), and one-way ANOVA test (**G**, **H**) were used to determine statistical significance. Data are reported as mean ± SD. $^*P < 0.05$; $^{**}P < 0.01$.

diminish the effect of S100A8/A9 on DC-mediated Th17 responses, and we found that the administration of anti–IL-23p19 prevented the production of IL-17 by $CD4^+$T cells co-cultured with S100A8/A9-treated DCs (Fig. 4E). Therefore, these data suggest that S100A8/A9 could promote the maturation of DCs and the expression of Th17-polarizing cytokines and pro-inflammatory chemokines in DCs.

Aconitate Decarboxylase 1 Is Involved in the Regulation of S100A8/A9 on DC Activation

To further elucidate the mechanism by which S100A8/A9 promotes DC activation, DCs treated with or without 4 µg/mL of S100A8/A9 were subjected to transcriptome sequencing analysis. By applying the criteria with a log fold change ≥ 2 and $P < 0.05$, significantly upregulated genes in four group of S100A8/A9-treated DCs relative to vehicle-treated DCs were filtered and subjected to a Venn diagram analysis, which revealed that 10 genes (*Cxcl3*, *Acod1*, *Oasl1*, *Rtp4*, *Irf7*, *Ifit1*, *Ifit1bl1*, *Il1b*, *Phf11a*, and *Ifit3b*) were upregulated simultaneously (Figs. 5A, 5B). These 10 genes were imported into the Search Tool for the Retrieval of Interacting Genes/Proteins (STRING) database (https://cn.string-db.org/), and the top three hub genes of a protein–protein interaction (PPI) network, including *Rtp4*, *Acod1* and *Oasl1*, were identified using the cytohubba plug-in for Cytoscape software (Fig. 5C). Among them, *Acod1* attracted our attention because of its critical role in regulating the antigen priming and effector function of DCs in type 2 airway inflammation.[32] qRT-PCR validation result showed that there was an about twofold increase in mRNA expression of *Acod1* in S100A8/A9-treated DCs (Fig. 5D). To clarify the role of *Acod1* in the regulation of S100A8/A9 on DC function, we silenced *Acod1* expression with siRNA in DCs prior to stimulation by S100A8/A9. Figure 5E shows the successful knockdown of *Acod1* by *Acod1*-specific siRNA, and Figures 5F to 5H demonstrate that the upregulation of *Il6* and *Il23a* mRNA induced by S100A8/A9, but not *Il1b*, was markedly reversed by *Acod1* silencing. These results suggest that *Acod1* is a key

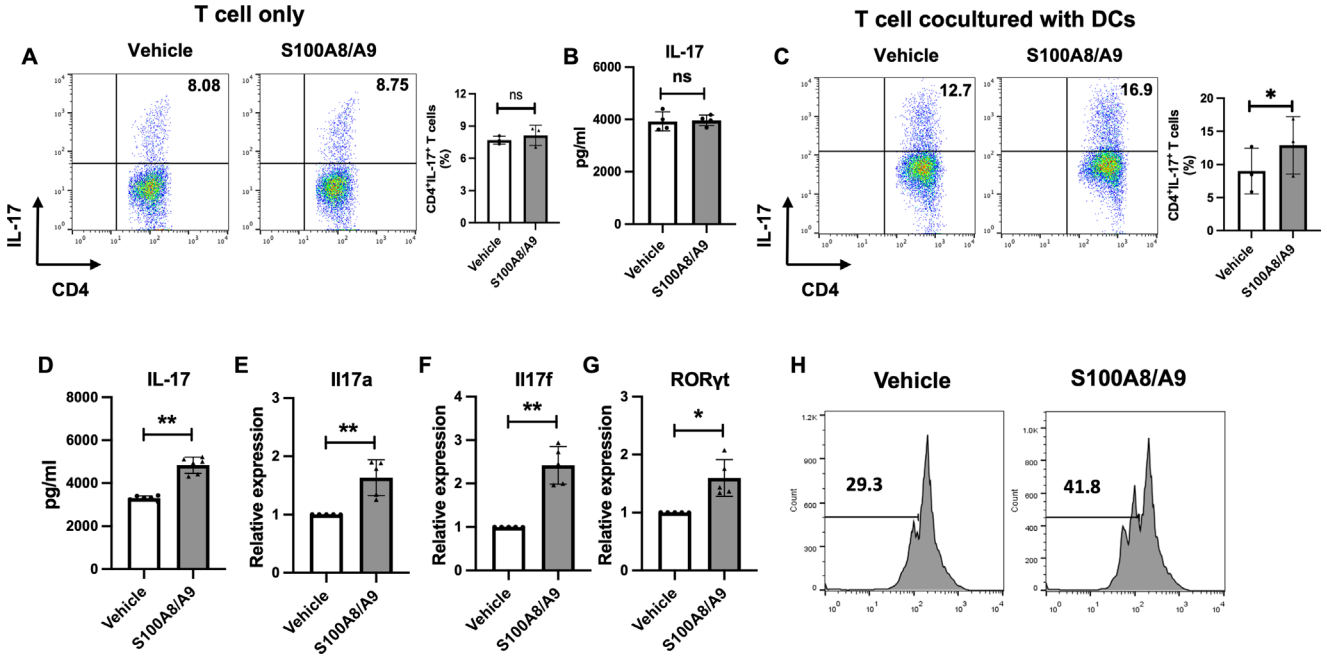

Figure 3. S100A8/A9 promotes DC-driven Th17 cell responses in vitro. (**A**, **B**) $CD4^+$T cells isolated from NOD mice were cultured in the presence or absence of recombinant S100A8/A9 protein (4 µg/mL) under Th17-polarizing conditions for 3 days (indicated by T cells only). Shown are representative flow cytometric plots (*left panel*) and percentages of $CD4^+IL\text{-}17^+$T cells (*right panel*) ($n = 3$) (**A**) and ELISA analysis for the secretion of IL-17 in the culture supernatants ($n = 4$) (**B**). (**C**–**G**) BMDCs were stimulated with or without recombinant S100A8/A9 protein for 24 hours and then co-cultured with $CD4^+$T cells sorted from NOD mice under Th17-polarizing conditions for 3 days (indicated by T cells co-cultured with DCs). Shown are representative flow cytometric plots (*left panel*) and percentages of $CD4^+IL\text{-}17^+$T cells (*right panel*) in the co-cultured systems ($n = 3$) (**C**); ELISA quantification of IL-17 levels in the supernatants of T cells co-cultured with S100A8/A9-treated and vehicle-treated DCs ($n = 6$) (**D**); and qRT-PCR analysis of the expression of Th17-related genes in the co-cultured cells ($n = 5$), including *Il17a* (E), *Il17f* (**F**), and *RORγt* (**G**). (**H**) Flow cytometry analysis of T-cell proliferation in two groups based on CFSE signals. Data in **A** to **G** were analyzed using two-tailed Student's *t*-test. Data are reported as mean ± SD. $^*P < 0.05$; $^{**}P < 0.01$; ns, no significance.

molecule mediating the promoting effect of S100A8/A9 on DC function.

S100A8/A9 Promotes the Activation of STAT3 Signaling Via *Acod1* in DCs

Among all members of the STAT family, STAT3 has been extensively documented to promote aberrant DC differentiation and function.[11] Here, we found that the upregulated genes in DCs upon S100A8/A9 stimulation were mainly enriched in the Janus kinase (JAK)/signal transducer and activator of transcription (STAT) and phosphoinositide-3-kinase (PI3K)/Akt signaling pathways (Supplementary Fig. S3A). Using western blot assays, we further observed that the levels of p-STAT3 in DCs were elevated in response to S100A8/A9 stimulation, whereas Akt phosphorylation remained unaffected (Fig. 6A), suggesting that S100A8/A9 may mainly affect STAT3 signaling. To validate this, we tested the expression of p-JAK2, the classical upstream signal of STAT3, and found that administration of S100A8/A9 also led to an increase in p-JAK2 levels in DCs (Fig. 6B). To further define whether *Acod1* was implicated in the regulation of S100A8/A9 on JAK2/STAT3 signaling, BMDCs were transfected with *Acod1* siRNA or control siRNA for 24 hours and exposed to S100A8/A9 for another 24 hours. Western blot showed that the upregulation of p-STAT3 induced by S100A8/A9 was counteracted by *Acod1* knockdown, whereas silencing *Acod1* had no effect on S100A8/A9-induced increases in JAK2 phosphorylation (Figs. 6C, 6D). Therefore, the above results demonstrate that *Acod1* may mediate the promoting effect of S100A8/A9 on the activation of STAT3 signaling.

Activation of STAT3 Signaling Contributes to the Promoting Effect of S100A8/A9 on DC-Driven Th17 Cell Responses by Inducing the Transcription of *Il23a*

To define whether STAT3 signaling was involved in the promoting effect of S100A8/A9 on DC-mediated Th17 cell responses, DCs pretreated with Stattic (a pharmacological inhibitor of STAT3 phosphorylation) were stimulated with S100A8/A9 and then co-cultured with $CD4^+$T cells isolated from NOD mice under Th17-polarizing conditions. As illustrated in Figures 7A and 7B, increased IL-17 production and $CD4^+IL\text{-}17^+$ T cell percentages induced by S100A8/A9-stimulating DCs were blocked by Stattic treatment, indicating the central role of STAT3 signaling in S100A8/A9-mediated promotion of Th17 cell responses through DCs. Further experiments revealed that inhibition of the STAT3 pathway by Stattic reversed S100A8/A9-mediated upregulation of MHC II and *Il23a* in DCs (Figs. 7C, 7F), whereas the increased expression of Il6 and Il1b in S100A8/A9-treated DCs was not significantly hindered by Stattic treatment (Figs. 7D, 7E).

Previous reports have implicated STAT3 as a key transcription factor that regulates the expression of pro-inflammatory genes.[33] Here, we observed that S100A8/A9

Investigative Ophthalmology & Visual Science

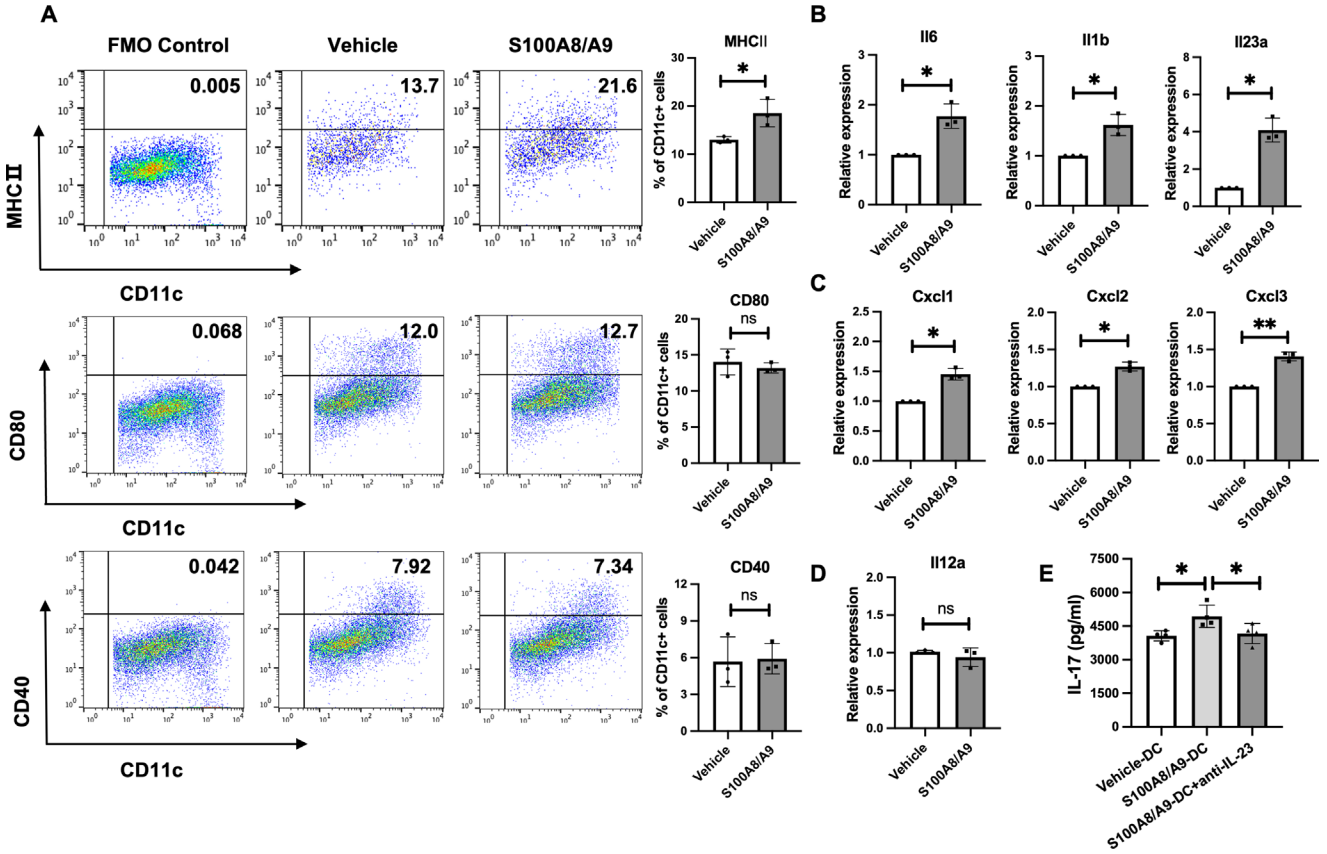

Figure 4. S100A8/A9 is responsible for the maturation and function of BMDCs. (**A**) Flow cytometric analysis and statistics of MHC II, CD80, and CD40 expression on BMDCs stimulated with or without recombinant S100A8/A9 protein ($n = 3$). (**B–D**) qRT-PCR analysis of gene expression, including proinflammatory cytokines (**B**, **D**) and chemokines (**C**) in vehicle-treated or S100A8/A9-treated BMDCs ($n = 3$). (**E**) DCs were treated with vehicle or recombinant S100A8/A9 protein for 24 hours and then co-cultured with $CD4^+$T cells in the presence or absence of anti-IL-23p19. Shown is the ELISA analysis of IL-17 levels in the supernatants of the coculture system ($n = 4$). Two-tailed Student's *t*-test (**A–C**), Mann–Whitney test (**D**), and one-way ANOVA test (**E**) were used to assess statistical significance. Data are reported as mean ± SD. $^*P < 0.05$; $^{**}P < 0.01$; ns, no significance.

induced the nuclear translocation of p-STAT3 in BMDCs (Fig. 7G). To investigate whether increased nuclear accumulation of p-STAT3 upon S100A8/A9 stimulation could promote the transcription of *Il23a*, we first analyzed publicly available STAT3 ChIP-seq data to assess the occupancy of STAT3 on the promoter region of *Il23a*. A significant enrichment of STAT3 was noted on the *Il23a* gene promoter region in BMDCs (Fig. 7H). Using a ChIP-PCR assay, we further verified that S100A8/A9-stimulating DC2.4 (mouse dendritic cell line) displayed increased p-STAT3 binding to Site 4 in the *Il23a* promoter region relative to vehicle-treated DC2.4 (Figs. 7I, 7J). Thus, these data demonstrate that the activation of STAT3 signaling is critically implicated in the promoting effect of S100A8/A9 on DC-driven Th17 cell responses by upregulating *Il23a*.

Administration of STAT3 Activator Counteracts the Repressive Effect of Paquinimod on the Development of SjDED

Because S100A8/A9 significantly promoted the activation of STAT3 in DCs, we proceeded to investigate the changes in p-STAT3 in LGs of WT and SjDED mice treated with paquinimod or vehicle. As presented in Figure 8A, the phosphorylation level of STAT3 was significantly increased in LGs of SjDED mice compared to the WT mice, whereas administration of paquinimod caused a significant decline in the phosphorylation of STAT3. In order to ascertain the role of p-STAT3 in S100A8/A9-induced autoimmunity in the context of SjDED, a STAT3 selective agonist, colivelin, was administered to SjDED mice as described in Figure 8B. Consistent with the results in Figures 2B and 2C, corneal fluorescein staining scores were markedly reduced in paquinimod-treated NOD mice compared with vehicle-treated mice, whereas colivelin treatment reversed this phenomenon (Figs. 8C, 8D). Furthermore, increased tear secretion in paquinimod-treated mice was also impeded after colivelin administration (Fig. 8E). Histologically, colivelin treatment increased the infiltration of inflammatory cells in LGs of paquinimod-treated mice (Fig. 8F). Also, decreased percentages of $CD11c^+$MHC II^+ cells and $CD4^+$IL-17^+ T cells in spleen and lymph nodes of paquinimod-treated SjDED mice were counteracted by colivelin treatment (Fig. 8G; Supplementary Figs. S4A, S4B). Collectively, our data support that paquinimod suppressed STAT3 to attenuate DC activation and Th17 cell response during the development of SjDED.

Discussion

In the present study, we explored the role of S100A8/A9 in the pathogenesis of SjDED and assessed the efficacy

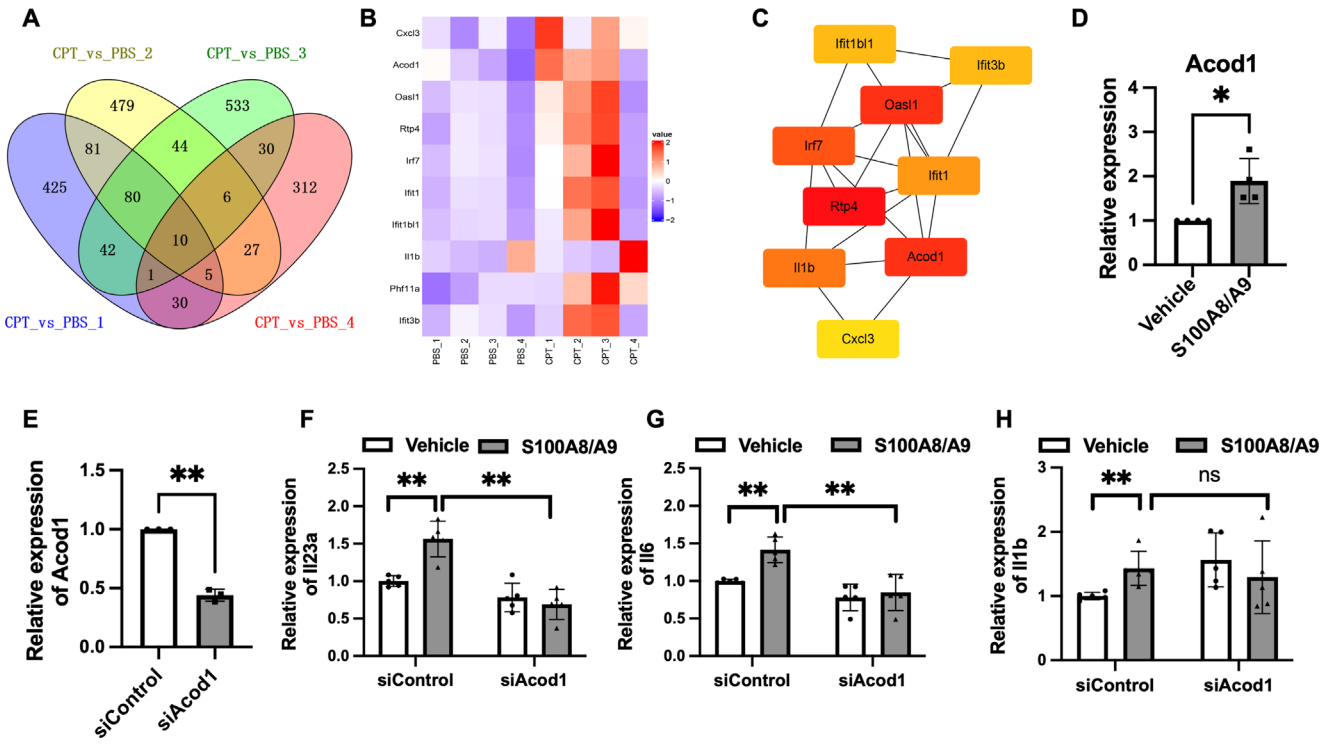

Figure 5. Acod1 is involved in the regulation of S100A8/A9 on DC function. (**A–C**) DCs were treated with recombinant S100A8/A9 protein (4 μg/mL) or vehicle for 4 hours and then subjected to RNA-seq analysis. Shown are a Venn diagram illustrating the overlapping upregulated genes in four groups of S100A8/A9-treated DCs compared with vehicle-treated DCs (CPT refers to calprotectin, which is also known as S100A8/A9) (**A**); an expression heatmap of the 10 overlapped genes indicated in **A** (**B**); and the hub-gene network of the overlapping genes identified by the cyto-Hubba plugin of Cytoscape software (**C**). (**D**, **E**) The mRNA expression of *Acod1* in S100A8/A9-treated or vehicle-treated DCs ($n = 4$) (**D**) and siAcod1- or siControl-transfected DCs ($n = 3$) (**E**) was analyzed by qRT-PCR. (**F–H**) DCs were transfected with siAcod1 or siControl for 24 hours and co-incubated with S100A8/A9 or vehicle for another 4 hours. The mRNA expression of *Il23a* (**F**), *Il6* (**G**), and *Il1b* (**H**) was determined by qRT-PCR ($n = 5$). Two-tailed Student's *t*-test was used for comparative analyses involving two groups (**D**, **E**). One-way ANOVA test was used for analyses involving more than two groups (**F–H**). All data are reported as mean ± SD. $^{*}P < 0.05$; $^{**}P < 0.01$; ns, no significance.

of S100A8/A9 blockade with paquinimod for the treatment of SjDED. We showed that elevated S100A8/A9 levels in PBMCs of SjDED patients were significantly associated with the increased OSDI scores and decreased tear secretion. Furthermore, in a mouse model of SjDED, the LGs displayed increased S100A8/A9 levels with disease progression. S100A8/A9 blockade could alleviate the development of DED with a significant reduction of Th17 cell frequency in LGs, spleens, and lymph nodes of SjDED mice. Further experiment demonstrated that S100A8/A9 induced the maturation and activation of DCs through the Acod1/STAT3 pathway and promoted DC-driven Th17 cell responses in SjDED mice (Fig. 8H). Therefore, our study has identified S100A8/A9 as a key driving factor in SjDED development and a potential treatment target for SjDED.

S100A8 and S100A9 have been studied in various diseases, such as cancers,[34,35] psoriasis,[23,36–38] diabetic nephropathy,[39] rheumatoid arthritis,[40,41] systemic lupus erythematosus,[42–44] and SjD,[45,46] In this study, we focused on the role of S100A8/A9 in the pathogenesis of SjDED, which has not yet been reported. Our findings that S100A8/A9 is upregulated in PBMCs of SjDED patients are consistent with previous results obtained in SjD and other autoimmune diseases.[43,45,46] The association among S100A8/A9, DED, and SjDED has also been observed. It has been shown that S100A8/A9 levels were significantly elevated in the tear fluids of patients with DED, and higher levels of S100A8/A9 were associated with more severe DED.[47] In line with this study, our results also revealed that the upregulation of S100A8/A9 in PBMCs of SjDED patients exhibited a significantly positive correlation with the OSDI scores as well as a negative correlation with the tear secretion levels. Furthermore, analysis of the GEO dataset (GSE176510) proved that there was a significant increase of S100A8/A9 in the conjunctiva of patients with SjDED.[19] Corroborating these findings in humans, the dynamic change of S100A8/A9 in NOD mice revealed that the expression of S100A8/A9 in LGs gradually increased with the progression of SjDED, and the levels of S100A8/A9 exhibited a positive correlation with the extent of lymphocyte infiltration in LGs, suggesting that S100A8 and S100A9 have the potential to serve as promising biomarkers for SjDED progression. Our results are further supported by a recent finding that S100A8 and S100A9 expression was upregulated with increasing age in splenic myeloid-derived suppressor cells of MRL/lpr mice, a well-known mouse model of systemic autoimmunity with SjD-like features.[44] More clinical samples should also be collected to further verify the possibility of using S100A8/A9 as a diagnostic marker for SjDED in the future.

IL-17–producing Th17 cells expressing the lineage-specific transcription factor RORγt are central to the pathogenesis of SjDED.[11] In this study, we observed that the administration of S100A8/A9 inhibitor reduced the infiltration and percentages of Th17 cells in the LGs, spleens,

Investigative Ophthalmology & Visual Science

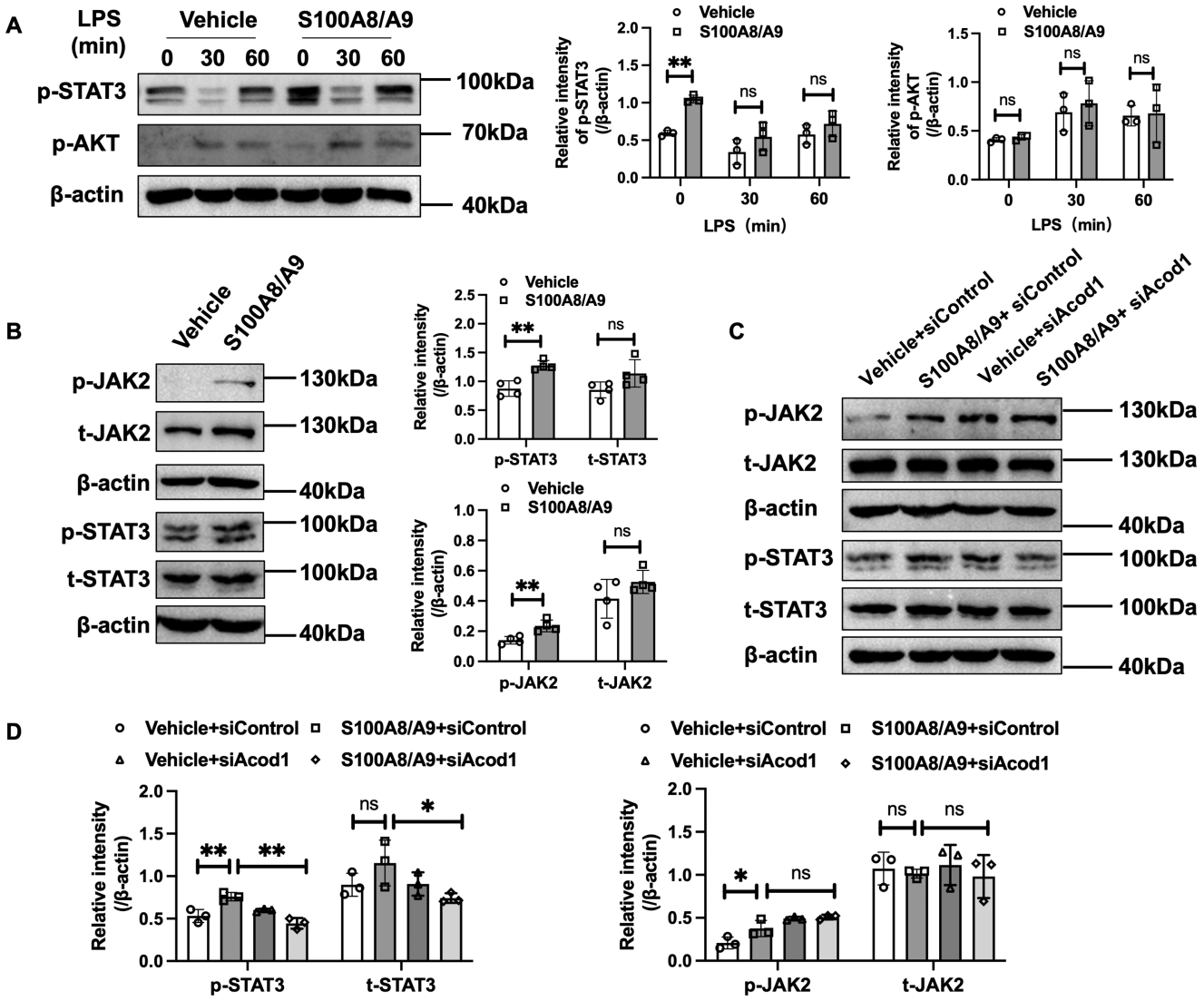

Figure 6. S100A8/A9 promotes Acod1-induced activation of STAT3 signaling in DCs. (**A**) Immunoblot analysis of p-STAT3 and p-AKT in S100A8/A9-treated or vehicle-treated DCs on the indicated time points after LPS stimulation ($n = 3$). (**B**) Immunoblot analysis of p-JAK2, total JAK2 (t-JAK2), p-STAT3, and total-STAT3 (t-STAT3) in protein extracts of DCs treated with S100A8/A9 or vehicle ($n = 4$). (**C**, **D**) Representative immunoblot (**C**) and quantitative analysis (**D**) of p-JAK2, t-JAK2, p-STAT3, and t-STAT3 in DCs transfected with siAcod1 or siControl for 24 hours followed by S100A8/A9 (4 µg/mL) stimulation for 24 hours ($n = 3$). Data in **A** and **B** were analyzed using two-tailed Student's *t*-test or Mann–Whitney test. Data in **D** were analyzed using one-way ANOVA test. Data are reported as mean ± SD. $^{*}P < 0.05$; $^{**}P < 0.01$; ns, no significance.

and lymph nodes of mice with SjDED, but in vitro results showed that S100A8/A9 treatment did not affect the generation of Th17 cells and IL-17 secretion. This hints that the inhibitory effect of S100A8/A9 blockade on Th17 cells in vivo was not due to direct regulation on T cells. DCs have been considered critical for the generation and activation of Th17 cells through secretion of cytokines, chemokines, and other proinflammatory molecules.[48] Recently, a study reported that S100A8- and S100A9-stimulated DCs exhibited an increased production of IL-23.[38] Consistent with this, we noticed that S100A8/A9 could enhance the expression of MHC II, Th17-polarizing cytokines (*Il23a*, *Il6*, and *Il1b*), and chemokines (*Cxcl1*, *Cxcl2*, and *Cxcl3*) in BMDCs, indicating that S100A8/A9 was involved in the regulation of DC maturation and function. Based on these findings, we speculated that S100A8/A9 may act on DCs to create a favorable milieu, which subsequently promoted Th17 differentiation and function. Indeed, we observed not only increased proportions of Th17 cells and IL-17 secretion but also significantly upregulated Th17 cell signature genes such as *Il17a*, *Il17f*, and *RORγt* in T cells co-cultured with S100A8/A9-treated DCs, suggesting the pivotal role of S100A8/A9 in DC-driven Th17 cell development and function. Our results are further supported by a previous report demonstrating that S100A8 did not increase IL-17 expression in naïve or activated $CD4^{+}$T cells but promoted IL-6 production in rheumatoid arthritis fibroblast-like synoviocytes to promote Th17 differentiation in rheumatoid arthritis.[49]

Acod1, a mitochondrial enzyme that catalyzes the production of itaconate, was originally identified as a lipopolysaccharide (LPS)-inducible gene involved in innate immunity in macrophages.[50] Recently, it has been demonstrated that the upregulation of *Acod1* expression in immune cells plays

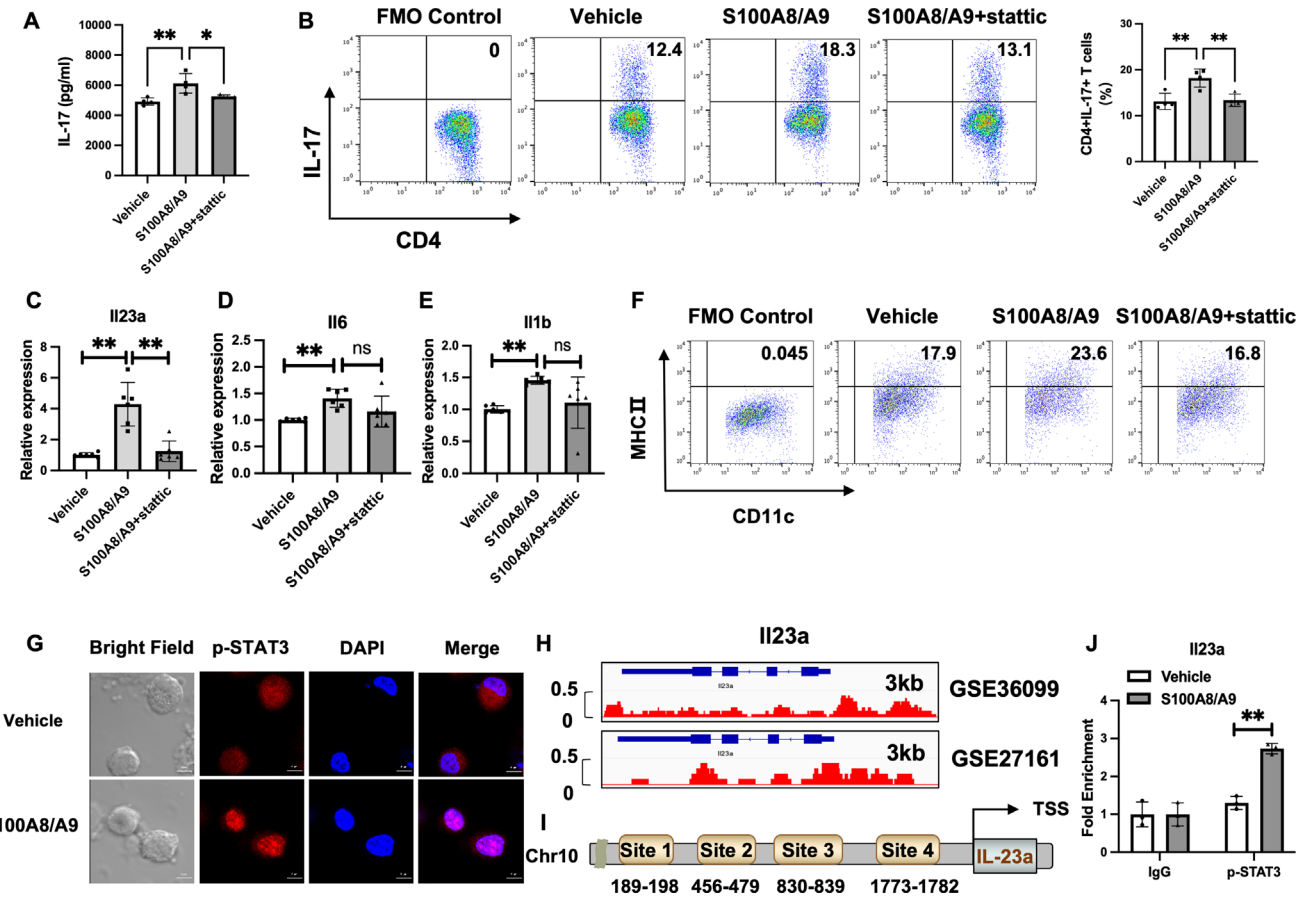

Figure 7. The activation of STAT3 signaling contributes to the promoting effect of S100A8/A9 on DC-driven Th17 cell responses by inducing the transcription of *Il23a*. (**A**, **B**) DCs were pretreated with Stattic (a STAT3 inhibitor) or DMSO for 1 hour followed by stimulation with S100A8/A9 and then co-cultured with $CD4^+$T cells under Th17-polarizing conditions. Shown are ELISA quantification of IL-17 in the supernatant of co-cultured cells ($n = 4$) (**A**) and flow cytometric analysis of the percentages of $CD4^+IL\text{-}17^+$T cells in the co-cultured cells ($n = 4$) (**B**). (**C**–**E**) qRT-PCR analysis of relative mRNA expression of *Il23a* (**C**), *Il6* (**D**) and *Il1b* (**E**) in S100A8/A9-stimulated DCs pretreated with or without Stattic ($n = 6$). (**F**) Representative flow cytometry plots of $CD11c^+MHC\ II^+$ cells in vehicle-treated, S100A8/A9-treated, and S100A8/A9 plus Stattic-treated DCs. (**G**) Representative images of immunofluorescence staining for p-STAT3 in S100A8/A9-treated or vehicle-treated DCs. *Scale bar*: 5 µm. (**H**) STAT3 occupancy on the *Il23a* locus in BMDCs through analysis of the published ChIP-seq databases (GSE36099 and GSE27161). (**I**) Schematic diagram of predicted STAT3 binding sites in the *Il23a* promoter region. (**J**) ChIP-qPCR analysis of the enrichment of p-STAT3 in the *Il23a* promoter region in DC2.4 treated with S100A8/A9 or vehicle ($n = 3$). One-way ANOVA test (**A**, **B**, **D**), Kruskal–Wallis test (**C**, **E**), and two-tailed Student's *t*-test (**J**) were used. Data are reported as mean ± SD. $^*P < 0.05$; $^{**}P < 0.01$; ns, no significance.

an important role in metabolic reprogramming, signal transduction, and inflammatory regulation.[51] By RNA-seq and qRT-PCR validation, we observed that the mRNA expression level of *Acod1* was markedly upregulated in S100A8/A9-treated DCs in comparison to vehicle-treated DCs, and knockdown of *Acod1* could weaken the promotion of S100A8/A9 on *Il6* and *Il23a* expression, indicating that *Acod1* may be required for S100A8/A9-induced upregulation of Th17-polarizing cytokines in DCs. Our further mechanistic study showed that S100A8/A9 facilitated activation of the JAK2/STAT3 signaling pathway in DCs, which is consistent with a recent study revealing that the phosphorylation levels of JAK2 and STAT3 were significantly increased in human endometrial stromal cells treated with S100A8/A9.[52] Notably, the promoting effect of S100A8/A9 on p-STAT3, rather than p-JAK2, was hindered in Acod1-silencing DCs, suggesting that Acod1 was responsible for S100A8/A9-induced activation of the STAT3 signaling pathway. Further studies are required to investigate the upstream regulator mediating S100A8/A9-induced activation of JAK2 in DCs.

Due to its important roles in immune cell activation and proinflammatory cytokine production, the STAT3 signaling pathway has been considered as a key player in the pathogenesis of DED.[53–55] Nevertheless, previous studies mainly focused on the regulation of STAT3 signaling on Th17 cells, so the potential impact of STAT3 signaling on DC activation and DC-mediated Th17 cell response remains poorly understood. Here, we found that S100A8/A9 enhanced *Il23a* transcription by inducing nuclear translocation of p-STAT3, and inhibition of p-STAT3 antagonized the increased expression of MHC II and *Il23a* induced by S100A8/A9 in DCs, indicating that the STAT3 pathway may be a crucial mediator in S100A8/A9-regulated DC-driven Th17 cell response through inducing the maturation of DCs and the expression of IL-23, a pivotal cytokine that drives the expansion and pathogenicity of Th17 cells.[56] Indeed, we observed the promoting effects of S100A8/A9-stimulating DCs on IL-17 production, and Th17 cell percentages were impeded after pretreatment with a STAT3 inhibitor. Supporting this, our in vivo data revealed that the administration of a STAT3

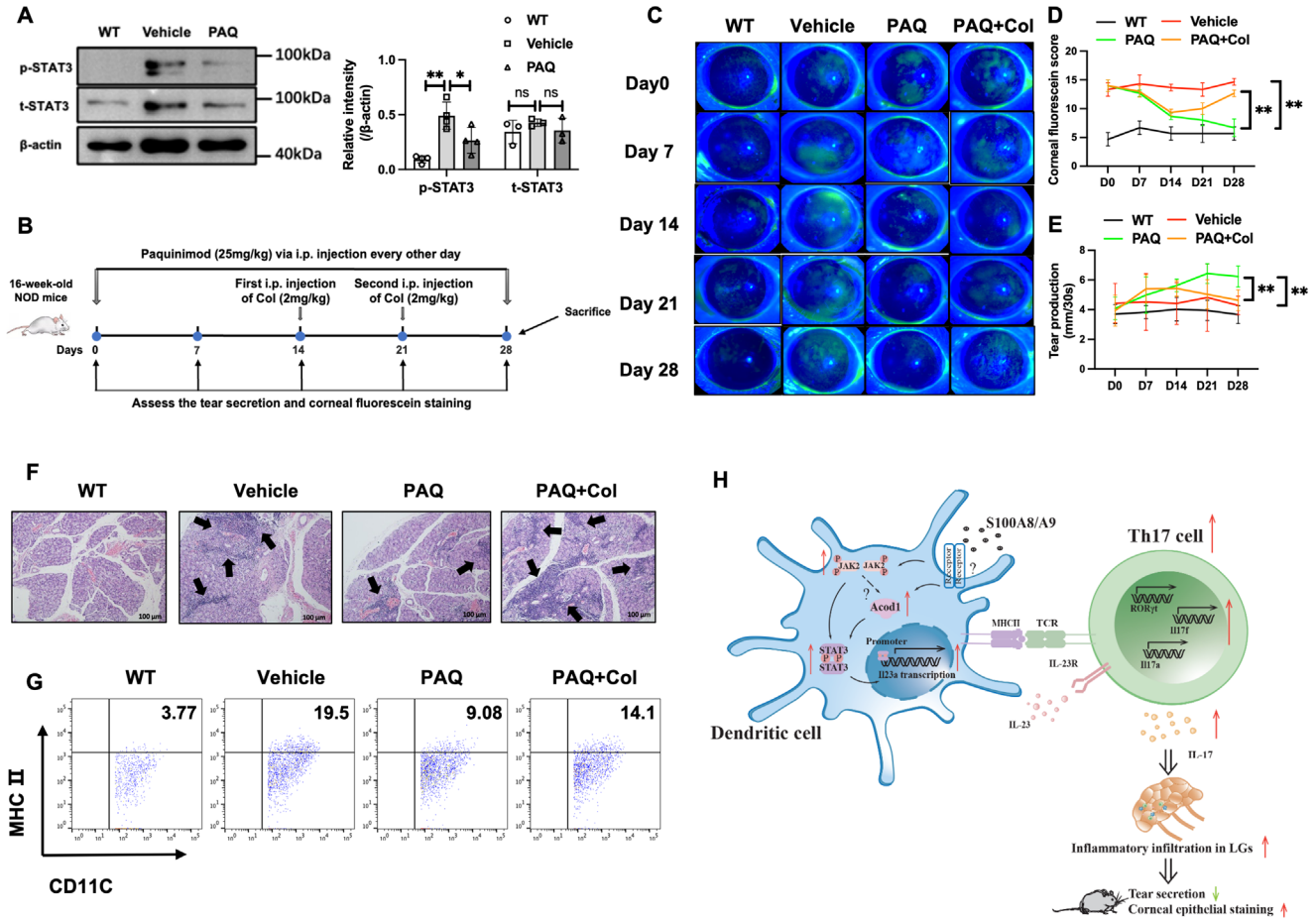

Figure 8. Administration of STAT3 activator reverses the therapeutic effect of paquinimod on SjDED. (**A**) Immunoblot analysis for the protein levels of p-STAT3 and t-STAT3 in LGs of WT mice and SjDED mice treated with paquinimod (PAQ) or vehicle (n = 3 or 4). (**B**) Schematic diagram showing the administration dose and schedule of PAQ and STAT3 activator colivelin (Col) in SjDED mice. (**C**, **D**) The representative images (**C**) and grading scores of corneal fluorescein staining (**D**) in WT, vehicle-, PAQ-, and PAQ plus Col-treated mice (n = 3). (**E**) Tear secretion measurement in WT mice (n = 3) and vehicle-, PAQ-, and PAQ plus Col-treated mice (n = 5). (**F**) Representative photomicrographs of H&E-stained LG sections showing the degree of inflammatory infiltration in WT mice and vehicle-, PAQ-, and PAQ plus Col-treated mice (n = 3). *Black arrows* represent foci of inflammatory cell infiltration. *Scale bars*: 100 µm. (**G**) The percentages of $CD11c^{+}MHC\ II^{+}$ cells measured by flow cytometry in splenic cells from WT mice and vehicle-, PAQ-, and PAQ plus Col-treated mice (n = 4). (**H**) The diagram displaying the mechanism underlying the regulation of S100A8/A9 on DC-driven Th17 cell response in the context of SjDED. S100A8/A9 upregulated Acod1 and p-JAK2 to induce the activation of STAT3 signaling, resulting in an increased transcription of *Il23a*, which promoted Th17 cell response and the development of SjDED. Data in **A** were analyzed using one-way ANOVA test, and data in **D** and **E** were analyzed using two-way ANOVA tests. Data are reported as mean ± SD. $^{*}P < 0.05$; $^{**}P < 0.01$; ns, no significance.

agonist restored decreased percentages of mature DCs and Th17 cells in paquinimod-treated NOD mice, further corroborating the pivotal role of STAT3 signaling in S100A8/A9-regulated Th17 cell responses and development of SjDED. However, additional mechanisms involved in the regulation of S100A8/A9 on DC-mediated Th17 cell responses in SjDED cannot be ruled out. For example, recent studies have reported that S100A8/A9 can activate nuclear factor kappa B (NF-κB) and MAPK signaling pathways to exacerbate the inflammation in rosacea, obesity, and spondyloarthritis.[57–59] In this study, we found that S100A8/A9 could also activate the JAK2 signaling pathway, but whether S100A8/A9 could regulate DC-driven Th17 cell responses via NF-κB, MAPK, or JAK2 signaling in SjDED remains to be further verified.

In summary, our study indicates that S100A8/A9 promotes the activation of DCs and DC-driven Th17 cell responses through the Acod1/STAT3 axis, thus contributing to the pathogenesis of SjDED. The S100A8/A9 inhibitor paquinimod successfully attenuated LG inflammation and improved clinical signs of DED in NOD mice. These findings may offer valuable insights for the therapy of SjDED by targeting S100A8/A9. Further studies are necessary to investigate whether the therapeutic effects of paquinimod on SjDED mice are long lasting and whether paquinimod can be applied to other types of Th17-mediated autoimmune diseases. Additional studies are also required to evaluate the pharmacodynamics of paquinimod in order to choose the optimal dosage and frequency for clinical treatment of patients with SjDED.

Acknowledgments

The authors thank the National Natural Science Foundation of China and Tianjin Health Research Project.

Supported by grants from the National Natural Science Foundation of China (82201157, 82070929), Tianjin Health Research

Project (TJWJ2024QN025), and Tianjin Key Medical Discipline (Specialty) Construction Project (TJYXZDXK-037A).

Disclosure: **Y. Wei**, None; **M. Sun**, None; **X. Zhang**, None; **C. Zhang**, None; **C. Yang**, None; **H. Nian**, None; **B. Du**, None; **R. Wei**, None

References

1. Ogawa Y. Sjögren's syndrome, non-Sjögren's syndrome, and graft-versus-host disease related dry eye. *Invest Ophthalmol Vis Sci*. 2018;59:DES71–DES79.
2. Ramos-Casals M, Brito-Zerón P, Bombardieri S, et al. EULAR recommendations for the management of Sjögren's syndrome with topical and systemic therapies. *Ann Rheum Dis*. 2020;79:3–18.
3. Wu KY, Chen WT, Chu-Bédard Y-K, Patel G, Tran SD. Management of Sjogren's dry eye disease-advances in ocular drug delivery offering a new hope. *Pharmaceutics*. 2022;15:147.
4. Chen Y, Dana R. Autoimmunity in dry eye disease – an updated review of evidence on effector and memory Th17 cells in disease pathogenicity. *Autoimmun Rev*. 2021;20:102933.
5. Zhao X, Li N, Yang N, et al. Thymosin $\beta 4$ alleviates autoimmune dacryoadenitis via suppressing Th17 cell response. *Invest Ophthalmol Vis Sci*. 2023;64:3.
6. Fan NW, Dohlman TH, Foulsham W, et al. The role of Th17 immunity in chronic ocular surface disorders. *Ocul Surf*. 2021;19:157–168.
7. Yin X, Chen S, Eisenbarth SC. Dendritic cell regulation of T helper cells. *Annu Rev Immunol*. 2021;39:759–790.
8. Cui X, Ye Z, Wang D, et al. Aryl hydrocarbon receptor activation ameliorates experimental colitis by modulating the tolerogenic dendritic and regulatory T cell formation. *Cell Biosci*. 2022;12:46.
9. Hilligan KL, Ronchese F. Antigen presentation by dendritic cells and their instruction of CD4+ T helper cell responses. *Cell Mol Immunol*. 2020;17:587–599.
10. Tiberio L, Del Prete A, Schioppa T, Sozio F, Bosisio D, Sozzani S. Chemokine and chemotactic signals in dendritic cell migration. *Cell Mol Immunol*. 2018;15:346–352.
11. Wang J, Wang J, Hong W, et al. Optineurin modulates the maturation of dendritic cells to regulate autoimmunity through JAK2-STAT3 signaling. *Nat Commun*. 2021;12:6198.
12. Guo Q, Zhao Y, Li J, et al. Induction of alarmin S100A8/A9 mediates activation of aberrant neutrophils in the pathogenesis of COVID-19. *Cell Host Microbe*. 2021;29:222–235.e4.
13. Li Y, Chen B, Yang X, et al. S100a8/a9 signaling causes mitochondrial dysfunction and cardiomyocyte death in response to ischemic/reperfusion injury. *Circulation*. 2019;140:751–764.
14. Skronska-Wasek W, Durlanik S, Le HQ, et al. The antimicrobial peptide S100A8/A9 produced by airway epithelium functions as a potent and direct regulator of macrophage phenotype and function. *Eur Respir J*. 2022;59:2002732.
15. Perumal N, Funke S, Pfeiffer N, Grus FH. Proteomics analysis of human tears from aqueous-deficient and evaporative dry eye patients. *Sci Rep*. 2016;6:29629.
16. Boehm N, Funke S, Wiegand M, Wehrwein N, Pfeiffer N, Grus FH. Alterations in the tear proteome of dry eye patients—a matter of the clinical phenotype. *Invest Ophthalmol Vis Sci*. 2013;54:2385–2392.
17. Sun YL, Cui AY, Wang LX, Zhang WW, Shi H. Dry environment on the expression of lacrimal gland S100A9, Anxa1, and Clu in rats via proteomics. *Int J Ophthalmol*. 2024;17:435–443.
18. Liang L, Yang X, Zeng H, et al. S100A9-TLR4 axis aggravates dry eye through the blockage of autophagy. *Exp Eye Res*. 2024;247:110052.
19. de Paiva CS, Trujillo-Vargas CM, Schaefer L, Yu Z, Britton RA, Pflugfelder SC. Differentially expressed gene pathways in the conjunctiva of Sjögren syndrome keratoconjunctivitis sicca. *Front Immunol*. 2021;12:702755.
20. Zhou L, Wei R, Zhao P, Koh SK, Beuerman RW, Ding C. Proteomic analysis revealed the altered tear protein profile in a rabbit model of Sjögren's syndrome-associated dry eye. *Proteomics*. 2013;13:2469–2481.
21. Loser K, Vogl T, Voskort M, et al. The Toll-like receptor 4 ligands Mrp8 and Mrp14 are crucial in the development of autoreactive $CD8^+$ T cells. *Nat Med*. 2010;16:713–717.
22. Yun J, Xiao T, Zhou L, et al. Local S100A8 levels correlate with recurrence of experimental autoimmune uveitis and promote pathogenic T cell activity. *Invest Ophthalmol Vis Sci*. 2018;59:1332–1342.
23. Defrêne J, Berrazouane S, Esparza N, et al. Deletion of S100a8 and S100a9 enhances skin hyperplasia and promotes the Th17 response in imiquimod-induced psoriasis. *J Immunol*. 2021;206:505–514.
24. Wolffsohn JS, Arita R, Chalmers R, et al. TFOS DEWS II Diagnostic Methodology report. *Ocul Surf*. 2017;15:539–574.
25. Shiboski CH, Shiboski SC, Seror R, et al. 2016 American College of Rheumatology/European League Against Rheumatism classification criteria for primary Sjögren's syndrome: a consensus and data-driven methodology involving three international patient cohorts. *Ann Rheum Dis*. 2017;76:9–16.
26. Xiao X, Luo P, Zhao H, et al. Amniotic membrane extract ameliorates benzalkonium chloride-induced dry eye in a murine model. *Exp Eye Res*. 2013;115:31–40.
27. Debreceni IL, Chimenti MS, Serreze DV, Geurts AM, Chen YG, Lieberman SM. Toll-like receptor 7 is required for lacrimal gland autoimmunity and type 1 diabetes development in male nonobese diabetic mice. *Int J Mol Sci*. 2020;21:9478.
28. Allred MG, Chimenti MS, Ciecko AE, Chen YG, Lieberman SM. Characterization of type I interferon-associated chemokines and cytokines in lacrimal glands of nonobese diabetic mice. *Int J Mol Sci*. 2021;22:3767.
29. Inaba K, Inaba M, Romani N, et al. Generation of large numbers of dendritic cells from mouse bone marrow cultures supplemented with granulocyte/macrophage colony-stimulating factor. *J Exp Med*. 1992;176:1693–1702.
30. Wei Y, Yang C, Liu Y, et al. Mettl3 induced miR-338-3p expression in dendritic cells promotes antigen-specific Th17 cell response via regulation of Dusp16. *FASEB J*. 2023;37:e23277.
31. Sun M, Wei Y, Zhang C, Nian H, Du B, Wei R. Integrated DNA methylation and transcriptomics analyses of lacrimal glands identify the potential genes implicated in the development of Sjögren's syndrome-related dry eye. *J Inflamm Res*. 2023;16:5697–5714.
32. Jaiswal AK, Yadav J, Makhija S, et al. Irg1/itaconate metabolic pathway is a crucial determinant of dendritic cells immune-priming function and contributes to resolute allergen-induced airway inflammation. *Mucosal Immunol*. 2022;15:301–313.
33. Zhang H, Hu H, Greeley N, et al. STAT3 restrains RANK- and TLR4-mediated signalling by suppressing expression of the E2 ubiquitin-conjugating enzyme Ubc13. *Nat Commun*. 2014;5:5798.
34. Chen Y, Ouyang Y, Li Z, Wang X, Ma J. S100A8 and S100A9 in cancer. *Biochim Biophys Acta Rev Cancer*. 2023;1878:188891.

35. Zhang X, Niu M, Li T, et al. S100A8/A9 as a risk factor for breast cancer negatively regulated by DACH1. *Biomark Res*. 2023;11:106.
36. Mellor LF, Gago-Lopez N, Bakiri L, et al. Keratinocyte-derived S100A9 modulates neutrophil infiltration and affects psoriasis-like skin and joint disease. *Ann Rheum Dis*. 2022;81:1400–1408.
37. Schonthaler HB, Guinea-Viniegra J, Wculek SK, et al. S100A8-S100A9 protein complex mediates psoriasis by regulating the expression of complement factor C3. *Immunity*. 2013;39:1171–1181.
38. Silva de Melo BM, Veras FP, Zwicky P, et al. S100A9 drives the chronification of psoriasiform inflammation by inducing IL-23/type 3 immunity. *J Invest Dermatol*. 2023;143:1678–1688.e8.
39. Du L, Chen Y, Shi J, et al. Inhibition of S100A8/A9 ameliorates renal interstitial fibrosis in diabetic nephropathy. *Metabolism*. 2023;144:155376.
40. Inciarte-Mundo J, Frade-Sosa B, Sanmartí R. From bench to bedside: calprotectin (S100A8/S100A9) as a biomarker in rheumatoid arthritis. *Front Immunol*. 2022;13:1001025.
41. von Wulffen M, Luehrmann V, Robeck S, et al. S100A8/A9-alarmin promotes local myeloid-derived suppressor cell activation restricting severe autoimmune arthritis. *Cell Rep*. 2023;42:113006.
42. Lood C, Tydén H, Gullstrand B, et al. Platelet-derived S100A8/A9 and cardiovascular disease in systemic lupus erythematosus. *Arthritis Rheumatol*. 2016;68:1970–1980.
43. Muñoz-Grajales C, Barraclough ML, Diaz-Martinez JP, et al. Serum S100A8/A9 and MMP-9 levels are elevated in systemic lupus erythematosus patients with cognitive impairment. *Front Immunol*. 2023;14:1326751.
44. Yang Y, Zhang X, Jing L, et al. MDSC-derived S100A8/9 contributes to lupus pathogenesis by promoting TLR7-mediated activation of macrophages and dendritic cells. *Cell Mol Life Sci*. 2024;81:110.
45. Nicaise C, Weichselbaum L, Schandene L, et al. Phagocyte-specific S100A8/A9 is upregulated in primary Sjögren's syndrome and triggers the secretion of pro-inflammatory cytokines in vitro. *Clin Exp Rheumatol*. 2017;35:129–136.
46. Tian Q, Zhao H, Ling H, et al. Poly(ADP-ribose) polymerase enhances infiltration of mononuclear cells in primary Sjögren's syndrome through interferon-induced protein with tetratricopeptide repeats 1-mediated upregulation of CXCL10. *Arthritis Rheumatol*. 2020;72:1003–1012.
47. Zhou L, Beuerman RW, Chan CM, et al. Identification of tear fluid biomarkers in dry eye syndrome using iTRAQ quantitative proteomics. *J Proteome Res*. 2009;8:4889–4905.
48. Lai W, Cai Y, Zhou J, et al. Deficiency of the G protein Gαq ameliorates experimental autoimmune encephalomyelitis with impaired DC-derived IL-6 production and Th17 differentiation. *Cell Mol Immunol*. 2017;14:557–567.
49. Lee DG, Woo JW, Kwok SK, Cho ML, Park SH. MRP8 promotes Th17 differentiation via upregulation of IL-6 production by fibroblast-like synoviocytes in rheumatoid arthritis. *Exp Mol Med*. 2013;45:e20.
50. Wu R, Liu J, Tang D, Kang R. The dual role of ACOD1 in inflammation. *J Immunol*. 2023;211:518–526.
51. Lang R, Siddique M. Control of immune cell signaling by the immuno-metabolite itaconate. *Front Immunol*. 2024;15:1352165.
52. Xin X, Liu H, Zhang S, et al. S100A8/A9 promotes endometrial fibrosis via regulating RAGE/JAK2/STAT3 signaling pathway. *Commun Biol*. 2024;7:116.
53. Stevenson W, Sadrai Z, Hua J, et al. Effects of topical Janus kinase inhibition on ocular surface inflammation and immunity. *Cornea*. 2014;33:177–183.
54. Liew SH, Nichols KK, Klamerus KJ, Li JZ, Zhang M, Foulks GN. Tofacitinib (CP-690,550), a Janus kinase inhibitor for dry eye disease: results from a phase 1/2 trial. *Ophthalmology*. 2012;119:1328–1335.
55. Qu M, Qi X, Wang Q, et al. Therapeutic effects of STAT3 inhibition on experimental murine dry eye. *Invest Ophthalmol Vis Sci*. 2019;60:3776–3785.
56. He L, Zhu X, Yang Q, et al. Low serum IL-17A in pregnancy during second trimester is associated with an increased risk of subclinical hypothyroidism. *Front Endocrinol (Lausanne)*. 2020;11:298.
57. Le Y, Zhang J, Lin Y, Ren J, Xiang L, Zhang C. S100A9 exacerbates the inflammation in rosacea through Toll-like receptor 4/MyD88/NF-κB signaling pathway. *J Invest Dermatol*.. 2024;144:1985–1993.e1.
58. Franz S, Ertel A, Engel KM, Simon JC, Saalbach A. Overexpression of S100A9 in obesity impairs macrophage differentiation via TLR4-NFkB-signaling worsening inflammation and wound healing. *Theranostics*. 2022;12:1659–1682.
59. Arias JL, Funes SC, Blas R, et al. S100A8 alarmin supports IL-6 and metalloproteinase-9 production by fibroblasts in the synovial microenvironment of peripheral spondyloarthritis. *Front Immunol*. 2022;13:1077914.

Investigative Ophthalmology & Visual Science